Hindawi
Advances in Materials Science and Engineering
Volume 2020, Article ID 6975968, 12 pages
https://doi.org/10.1155/2020/6975968

Research Article

Evolution of the Electrical Displacement and Energy Dissipation of Lead Zirconate-Titanate Ceramics under Cyclical Load

Sheng Cang[1,2], **Jiankang Chen**[1] and **Chunsheng Lu**[3]

[1]*The Faculty of Mechanical Engineering and Mechanics, Ningbo University, Ningbo 315211, China*
[2]*Ningbo City College of Vocational Technology, Ningbo 315100, China*
[3]*School of Civil and Mechanical Engineering, Curtin University, Perth, WA 6845, Australia*

Correspondence should be addressed to Jiankang Chen; chenjiankang1957@163.com and Chunsheng Lu; c.lu@curtin.edu.au

Received 26 January 2020; Accepted 3 March 2020; Published 24 March 2020

Academic Editor: Tetsu Yonezawa

In this paper, the electromechanical behavior of lead zirconate-titanate ceramics (P51) has been characterized and modeled. The variation of the energy dissipation and peak electrical displacement of the P51 ceramic has been investigated in details. The total strain of P51 under cyclical loading consists of elastic deformation (ε_{ij}^{e}), immediate ferroelectric domain switching deformation (ε_{ij}^{d}), and time-dependent deformation (ε_{ij}^{c}). Thus, an expression for the energy dissipation of P51 can be theoretically derived. In addition, a practical method for calculating the dissipated energy has been proposed by integrating the curve of a hysteresis loop. The experimental results show that the peak electrical displacement and dissipated energy both decrease monotonously with the increase of the number of cycles. Furthermore, ferroelectric 90° domain switching was observed by X-ray diffraction (XRD) and the percentage of domain switching has been calculated by the variation of the peak intensity ratio of (002) to (200) at about 45 degrees. Then, grain debonding, crack, and crush were found around voids inside the specimen by using scanning electron microscope (SEM). It is indicated that switching of more capable-switch domains stimulates larger dissipated energy and a bigger peak electrical displacement at the initial cyclic loading. Finally, an exponential functional model has been proposed to simulate the peak evolution of electrical displacement based on the energy dissipation of P51 ceramics under cyclical load.

1. Introduction

Due to their excellent electromechanical coupling ability, lead zirconate-titanate ceramics have been widely used as actuators and sensors [1–4] for health monitoring of large and complex structures, as well as functional materials for environmental power generation [5–7]. However, degradation of their electromechanical properties generally limits the application of piezoelectric ceramic materials. Until now, the mechanism of degradation of piezoelectric properties has not been unified; the majority of researchers have attributed degradation to domain switching. Fritz [8] found that there were two effects of the rotation of ferroelectric domains and the ferroelectric to antiferroelectric phase transition under uniaxial-stress conditions in two modified lead zirconate-titanate ferroelectric ceramics. Similarly, Cao and Evans [9] and Lynch [10] observed the severe nonlinear and hysteretic behavior of piezoceramics, respectively, due to domain switching. Fan et al. [11] studied four different PZT composites under uniaxial compressive stress and a cyclical electric field. They discovered that switching initially behaved as a smooth softening process, which resulted in a large change of strain and electrical displacement, followed by a macroscopic saturation hardening process. As to under what conditions domain switching can happen, Calderon-Moreno [12] indicated that the 90° domain rotation associated with damage is stress-induced when exceeding the coercive stress of 60 MPa for soft PZT and 130 MPa for hard PZT. Moreover, Algueró et al. [13] investigated degradation of the piezoelectric coefficient of soft and hard PZT ceramics under static and cyclical compressive loading, and they showed that the soft material had significant piezoelectric degradation due to stress-induced depolarization in the range of 10 to 70 MPa, especially under cyclical loading. Okayasu et al. [14] studied the electromechanical properties of PZT ceramics and realized that the material hardening

occurred due to domain switching, which was clearly detected by the electron backscattered diffraction analysis (EBSD). Fang and Li [15] examined the effect of different compressive stress levels on the electromechanical response. The results showed that the electric-mechanical coupled properties of the PZT ceramic were the function of the compressive stress. However, being viscous and time-dependent is the special property of piezoceramic material on account of the preparation technique. Lente and Eiras [16] found that domain switching is dependent on loading frequency described as a viscoelastic process. Zhou and Kamlah [17] focused on the experimental investigation of time-dependent effects of piezoceramic material at room temperature and found the material exhibited the greatest time-dependent effects at a stress level near the coercive stress. Webber et al. [18] indicated that the nonlinear strain can be attributed to the domain wall motion and accompanying misfit strains surrounding switching domain. Furthermore, Pojprapai et al. [19] theoretically proposed a rheological model representing time-dependent deformation and separated the steady-state creep strain from transient creep strain macroscopically under the square wave cyclic loading.

With the development of measuring instruments, domain switching and zone have been observed around microcracks by Electron Backscatter Diffraction [14], X-ray diffraction [20, 21], atomic force microscope [22], and liquid crystal display techniques [23]. Finally, Schneider [24] demonstrated experimentally that the fracture toughness enhancement due to domain switching was strongly related to the crack growth of ferroelectric ceramics under electrical and mechanical loads.

Here, it is worth noting that, in all these research studies mentioned above, seldom literature was concentrated on the time-dependent property of piezoceramic material, which may be greatly affect not only the mechanical properties but also the electrical properties under cyclical loading.

In this paper, the concept of degradation of the electrical properties of piezoceramic material, denoted as peak electrical displacement, has been proposed as a function of energy dissipation consideration of time-dependent deformation. Then, the relationship has been discussed between energy dissipation and the peak electrical displacement under cyclical compression tests. The paper is organized as follows. Firstly, experimental methodology is introduced. Then, the results are systematically analyzed and discussed with an expression of the energy dissipation applied under a triangular stress. Here effects of the stress amplitude and loading rate have been investigated on the dissipated energy and peak electrical displacement in terms of microstructures. Subsequently, a model simulating the peak evolution of electrical displacement has been proposed based on the dissipated energy. Finally, the main conclusions are summarized.

2. Experimental Methodology

2.1. Materials and Specimen Preparation. The selected piezoceramic material is a commercial poled bulk lead zirconate-titanate ceramic (P51, produced by Baoding Hongsheng Acoustic Electronic Equipment Co., China), with the physical and electromechanical properties as listed in Table 1. The dimensions of specimens are $15 \times 15 \times 12\ \text{mm}^3$, and as shown in Figure 1, they were coated with silver on the top and bottom surfaces to act as electrodes. The polarization parallel to the height dimension is perpendicular to the electrodes. Small pieces cut from the specimen were detected by scanning electric microscope and X-ray diffraction, respectively. It is found that the grain size is about 3~5 μm and the microvoid size is about 5~8 μm (see Figure 2(a)). Furthermore, the X-ray diffraction pattern indicates that the specimen has a good crystallinity and pure perovskite structure, as well as the typical tetragonal phase structure below Curie temperature due to the two-peak structure at about 45 and 55 degrees (Figure (2b)).

2.2. Methods. By using the experimental setup, as illustrated in Figure 3(a), a uniaxial cyclical compression stress can be applied to the specimen. Here, the 810 material test system (MTS) frame employed to loading is a servohydraulic system that controls stress, strain, and displacement. Alumina blocks were used to electrically isolate the specimen from the test frame. Copper foil tape was attached to the bottom of alumina blocks and connected to the charge amplifier, and an extensometer was fixed to alumina blocks. The output data of both force and displacement were collected through the MTS frame, while the electrical displacement data were measured by a dynamic signal tester.

The cyclical compression stress was applied, parallel to the polarization direction of the specimen. Before testing, the specimen was firstly carefully put on the center of the bottom alumina block. Then, a small preload of 50 N was applied. Each cyclical load was divided into two stages: loading and unloading, as shown in Figure 3(b). Three stress amplitudes (σ_0) of 30, 65, and 100 MPa were applied to specimens under three different loading rates ($\mathrm{d}\sigma/\mathrm{d}t$) of 0.5, 1.0, and 1.5 MPa/s, respectively.

Meanwhile, the changes of piezoelectric effect (d_{33}) and microstructure of P51 specimen were conducted by a Berlincourt meter (IACAS, ZJ-3AN), XRD, and SEM after every cyclical load, respectively.

3. Results and Discussion

3.1. Energy Dissipation under Cyclical Load Test. Ferroelastic behavior can be separated into linear and nonlinear material response, as quantified in the following equation [18]:

$$\varepsilon_{ij} = \varepsilon_{ij}^{e} + \varepsilon_{ij}^{p}, \tag{1}$$

where ε_{ij} is the total strain and the superscripts e and p indicate the elastic and plastic contributions, respectively. Zhou and Kamlah [17] further illustrated that the plastic deformation includes two irreversible deformation: one is immediate ferroelectric domain switching deformation (ε_{ij}^{d}) and the other is time-dependent deformation (ε_{ij}^{c}). Hence, (1) can be described as

Table 1: The physical and electromechanical properties of P51.

Material	Density (kg/m^3)	Piezoelectric coefficients d_{33} (pC/N)	Relative dielectric constant ε	Mechanical quality factor Q_m	Curie temperature (°C)
P51	7500	450	2500	85	340

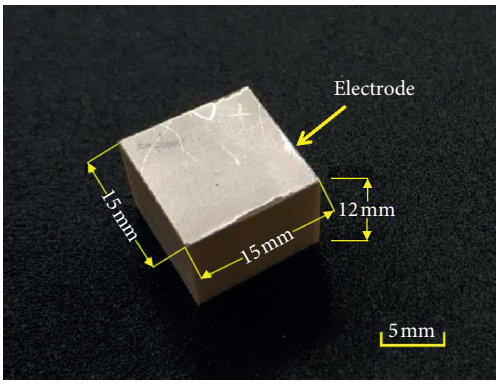

Figure 1: Photograph of a typical specimen of P51.

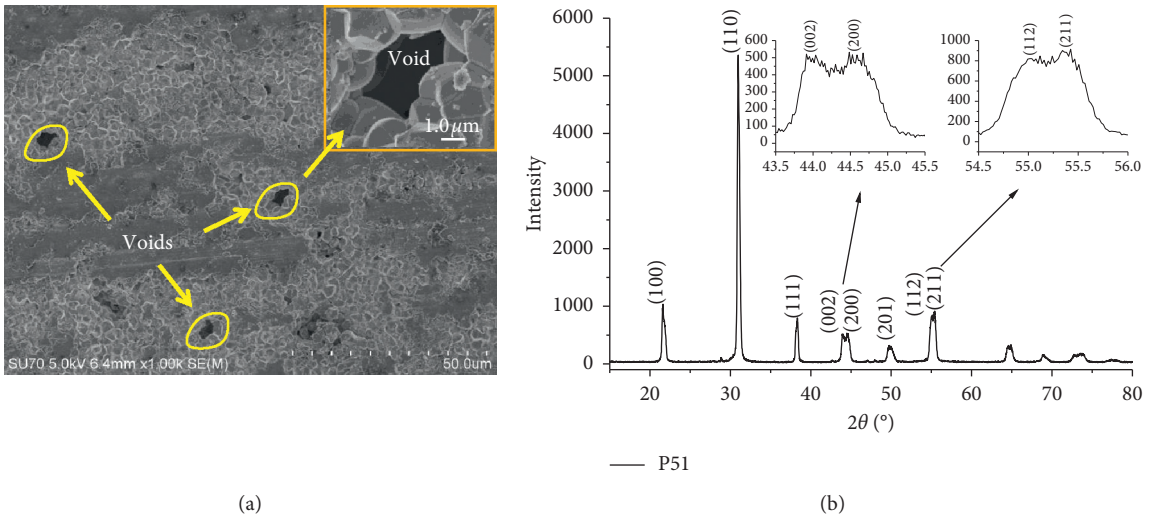

Figure 2: Photograph of (a) SEM and (b) X-ray diffraction pattern of P51.

$$\varepsilon_{ij} = \varepsilon_{ij}^{e} + \varepsilon_{ij}^{d} + \varepsilon_{ij}^{c}. \tag{2}$$

However, the incremental linear elastic response at zero electric field is shown as follows:

$$\Delta\varepsilon_{ij}^{e} = s_{ijkl}(\sigma, T)\Delta\sigma_{kl}, \tag{3}$$

where s_{ijkl} is the linear compliance ($s_{ijkl} = c_{ijkl}^{-1}$) at constant temperature (T) and σ_{kl} is the applied stress.

Webber et al. [18] separated the linear and nonlinear strain from the total and demonstrated that the nonlinear strain comprised approximately one-half of the total strain at maximum stress. Thus, the increment of the total strain energy applied compressive stress can be expressed as

$$\Delta W = \Delta\varepsilon_{ij} \cdot \Delta\sigma_{kl}. \tag{4}$$

Substituting (2) into (4) yields

$$\Delta W = \left(\Delta\varepsilon_{ij}^{e} + \Delta\varepsilon_{ij}^{d} + \Delta\varepsilon_{ij}^{c}\right) \cdot \Delta\sigma_{kl}. \tag{5}$$

During a complete loading process, (5) can be transformed as

$$\begin{aligned} W = W_e + W_d &= \int \left[\Delta\varepsilon_{ij}^{e} + \left(\Delta\varepsilon_{ij}^{d} + \Delta\varepsilon_{ij}^{c}\right)\right] \cdot \mathrm{d}\sigma_{kl} \\ &= \int s_{ijkl}(\sigma, T) \cdot \Delta\sigma_{kl} \cdot \mathrm{d}\sigma_{kl} + \int \left(\Delta\varepsilon_{ij}^{d} + \Delta\varepsilon_{ij}^{c}\right) \cdot \mathrm{d}\sigma_{kl}, \end{aligned} \tag{6}$$

where W_e and W_d are the elastic strain energy and the dissipated strain energy, respectively. Because the linear response is a reversible deformation, the elastic strain energy is equal to zero by applied cyclic load, as shown in

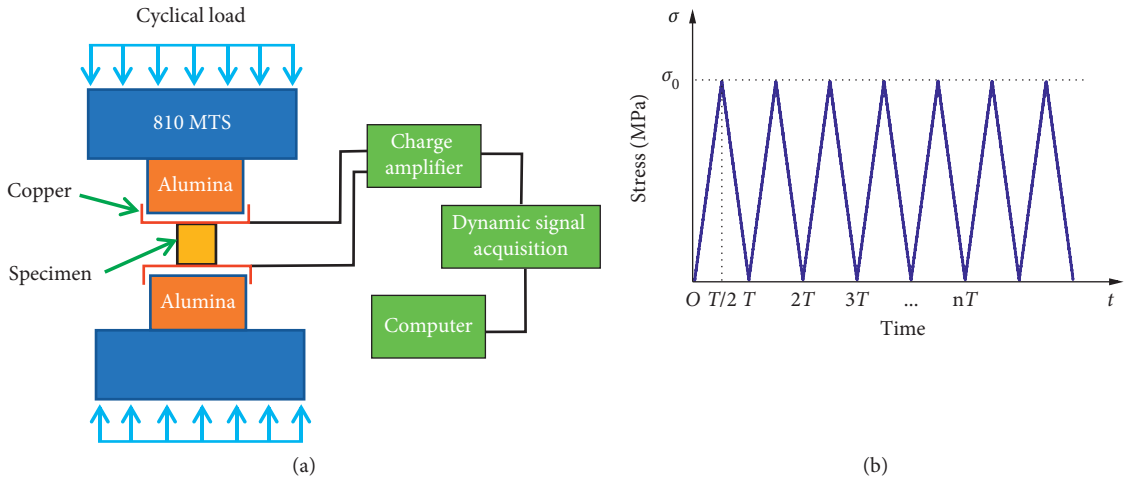

Figure 3: Illustration of (a) the experimental setup and (b) loading curve, where T indicates a loading period.

Figure 3(b). Therefore, the dissipated strain energy in one cyclic load can be shown as

$$W_d = W - W_e = \oint \left(\Delta\varepsilon_{ij}^d + \Delta\varepsilon_{ij}^c\right) \cdot d\sigma_{kl}. \tag{7}$$

Usually, it is difficult to distinguish ε_{ij}^d from ε_{ij}^c in triangle cyclic loading. Hence, a practical method to attain energy dissipation is adopted widely as illustrated in Figure 4 [25]. Here, the area of a hysteresis loop represents the dissipated energy in one cyclic loading, which is equal to the solution of (7) by subtracting W_e from W. Thus, the dissipated energy can be obtained by integrating the curve of a hysteresis loop, that is,

$$W_d = \sum_L \left(\sigma_i^L + \sigma_{i+1}^L\right) \cdot \frac{\left(\varepsilon_{i+1}^L - \varepsilon_i^L\right)}{2} - \sum_U \left(\sigma_i^U + \sigma_{i+1}^U\right) \cdot \frac{\left(\varepsilon_{i+1}^U - \varepsilon_i^U\right)}{2}, \tag{8}$$

where stresses of σ_i^L and σ_i^U, as well as strains of ε_i^L and ε_i^U, represent loading and unloading stages, respectively, which can be experimentally determined.

3.2. Effects of Stress Amplitude and Loading Rate on Energy Dissipation. It is obvious that the dissipated energy of seven cyclic loadings can be divided into two stages shown in Figure 5. One stage is the first and the second cyclic loading. There is a fast decrease of the energy dissipation from the first cyclic loading to the second. Then, the remanent cyclic loading showing a slow downward decrease is the second stage. Figure 5(a) indicated that larger stress amplitude represents larger dissipated energy. However, the dissipated energy apparently depended on the loading rate as a time-dependent material shown in Figure 5(b). Lower loading rate means longer time applied to the specimen and yields a larger time-dependent deformation.

In order to illustrate clearly the effect of stress amplitude and loading rate on energy dissipation, the variation of the dissipated energy of the first, second, and final cyclic loading with different stress amplitude and loading rate is plotted in Figure 6. From Figure 6(a), it is seen that all the dissipated

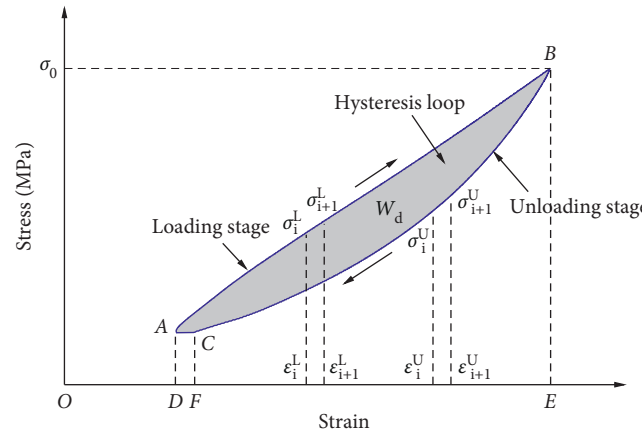

Figure 4: Schematic diagram of energy dissipation in a hysteresis loop.

energy increases with the increase of stress. In particular, the dissipated energy increases remarkably with the increase of stress in the first cycle. Then, the dissipated energy increases gently. Similarly, the dissipated energy is also affected by the loading rate applied under the same stress amplitude. In all the cases, the dissipated energy decreases with the increase of the loading rate. The decrement in each case is almost equal to the dissipated energy in each cycle. As is well known, the larger stress denotes a larger energy at the same loading rate. However, a higher loading rate results in a smaller dissipated energy, compared to that of a larger stress. This is because P51 ceramics are time-dependent materials [16–19], and strain would become larger under stress being held or even a constant. A lower loading rate denotes a longer duration on the specimen, which results in a larger energy at the same stress amplitude.

From (7), the energy dissipation consists of two parts: one is immediate ferroelectric domain switching deformation (ε_{ij}^d), and the other is time-dependent deformation (ε_{ij}^c). The deformation induced by domain switching depends on the quantity of switching-capable grains. Obviously, more domains switched at the first cyclic loading and attributed

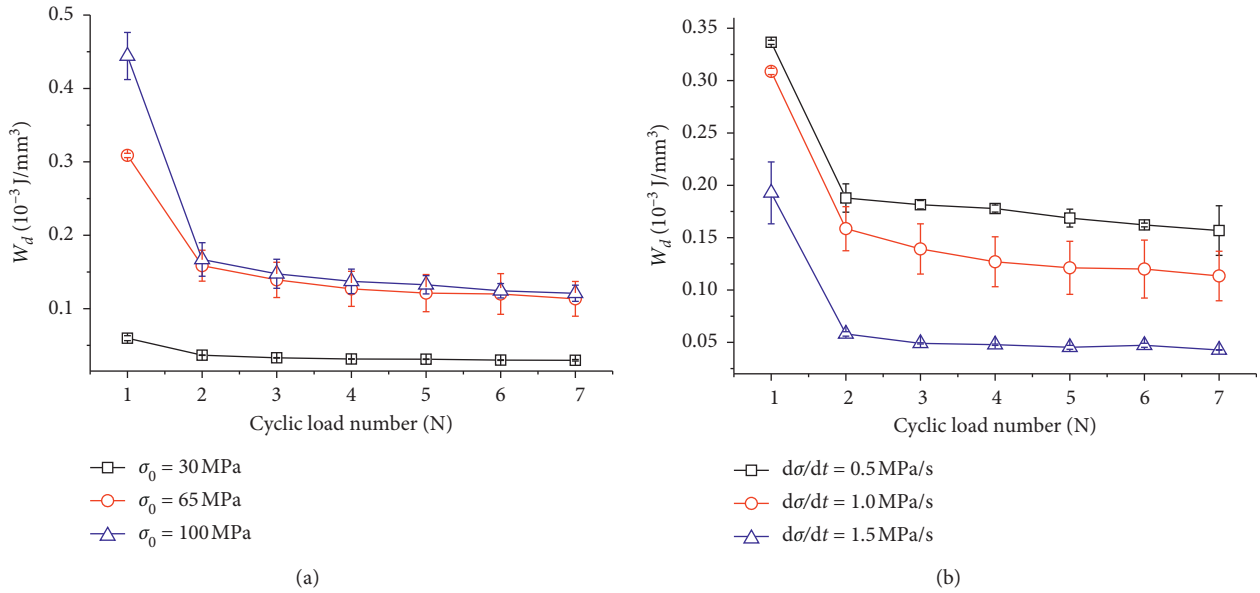

Figure 5: Dissipated energy per unit volume versus with the number of cycles. (a) dσ/dt = 1.0 MPa, and (b) σ_0 = 65 MPa.

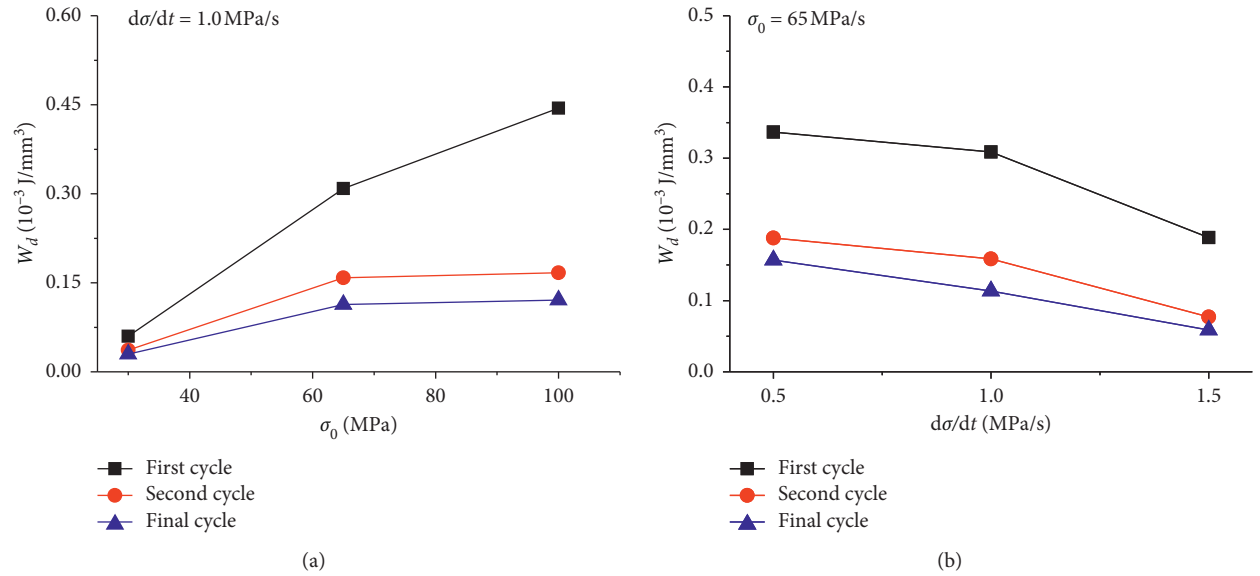

Figure 6: The dissipated energy during the 1st, 2nd, and final cycles versus with (a) σ_0 and (b) dσ/dt.

more deformation than that of the subsequent cyclic loading. As the cyclic loading going on, the switching-capable grains became less until no domain switching occur. On the other hand, the time-dependent deformation is only determined by duration time once the stress amplitude is determined. Hence, the dissipated energy is much larger at first cyclic loading than that at the subsequent cyclic loading. In the end, the dissipated energy decreased to a constant due to the main attribution of time-dependent deformation with no more domain switching.

3.3. Effects of Stress Amplitude and Loading Rate on Electrical Displacement. How the piezoelectric response to the applied triangle cyclic load can be described, as shown in Figure 7(a). At the beginning of loading, the electric displacement reaches the peak value as soon as the stress was applied. Then, electric displacement decreases sharply with the increase of applied stress. Until the end of loading, the electric displacement slows down closely to zero. When transferred to unloading, the electric displacement again reaches the peak value instantaneously in the opposite direction. With the increase of the applied stress, the electric displacement decreases fast and then slows down closely to zero until loading again.

After each cyclic load, the piezoelectric coefficient (d_{33}) of two specimens' variation with cyclic load number is plotted in Figure 7(b). The measured value of d_{33} before test

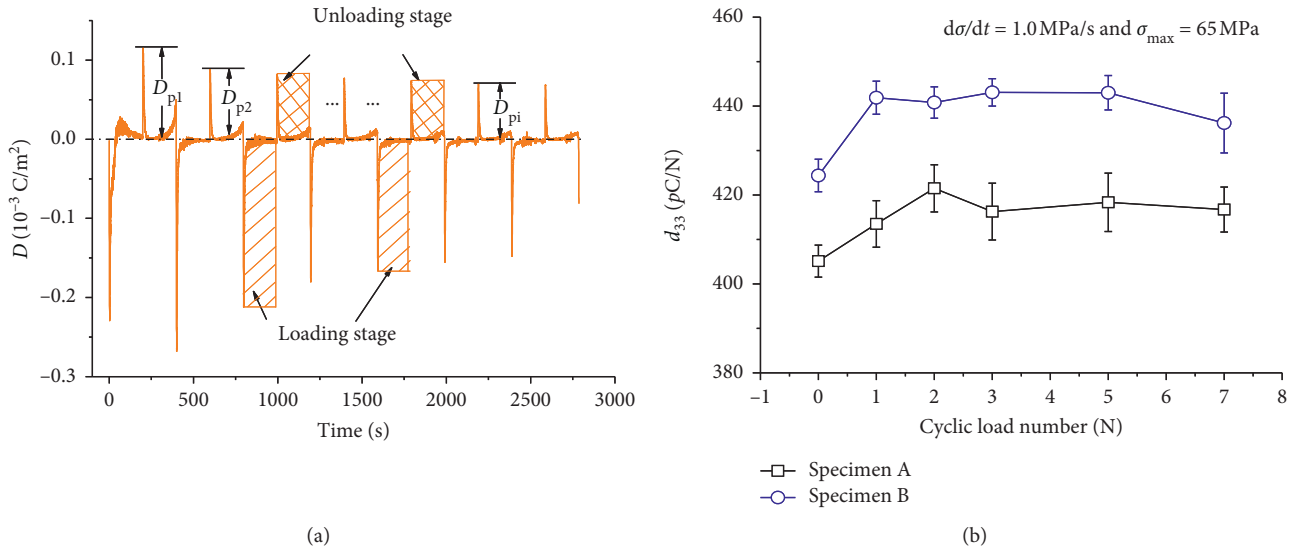

Figure 7: Schematic of (a) the electrical displacement versus with time and (b) d_{33} versus cyclic load number.

is smaller than the named value given in Table 1 due to aging [26]. Therefore, two interesting things should be paid more attention. One is the measured piezoelectric coefficient before test is smaller than that of the first cyclic loading. The increase of the piezoelectric coefficient after the first cyclic loading indicates that the depolarized piezoceramics may be poled with mechanical stress [27]. The other is that the piezoelectric coefficient began to drop from the beginning of the second cyclic loading. Algueró et al. [13] demonstrated experimentally that the piezoelectric coefficient can be measured as a function of the amplitude of the applied stress considering of the domain wall attribution and also found a significant piezoelectric degradation of soft piezoceramics due to stress-induced depolarization, while the piezoelectric degradation was not found in the hard piezoceramics (PZT-4D).

The mechanism of piezoelectric effect under cyclical load can be illustrated, as shown in Figure 8. The electric displacement curve ($\overline{ABCDE}$) induced by one cyclic load ($A'D'E'$) is plotted in Figure 8(a). At first, the poled piezoceramic appears to be neutral due to the bounded charges adsorbing the free charges at the surface perpendicular to the direction of polarization (Figure 8(b)A). When applying compression stress, the piezoceramic deforms and motivates a transient peak due to lots of charges transferring to the surface (Figure 8(b)B). Before transferring to unloading stage, the output charges drop fast and then slow downward to zero with the increase of stress (Figure 8(b)C). Once unloading, the inverse transient peak is motivated on account of the lots of charges transferring to the opposite crystal surface (Figure 8(b)D). Until loading again, the quantities of the output charges drop fast and then decrease gradually to zero (Figure 8(b)E).

Therefore, the peak electrical displacement in the unloading stage, denoted as D_{pi} (see Figure 7(a)), versus that with the number of cycles is given in Figure 9. It is of interest to note that, similar to the dissipated energy, the peak electrical displacement, D_{pi}, reduces sharply in the second cycle and decreases gradually to a constant in the subsequent cycles. The decrease of D_{pi} implies the degradation of the piezoelectric effect, which is probably induced by the degradation of either the piezoelectric coefficient [13] or permittivity [28] under cyclical compression loading.

Similarly, D_{pi} of the first, second, and final cyclic loading with different stress amplitude and loading rate are plotted in Figure 10. As shown in Figure 10(a), stress amplitude has a significant effect on the peak electrical displacement in the first cycle. Though the peak electrical displacement increases in the subsequent cycles, its increment slows down. Hence, the peak of electrical displacement does not consistently increase with the increment of stress amplitude.

On the other hand, the peak electrical displacement is sensitive to the loading rate. Li et al. [29] found that the amplitude of piezoelectric voltage was linear with the frequency of a cyclic load. The larger the loading rate in each cycle, the larger the peak value of an electrical displacement (see Figure 9(b)). Rapid recovery of deformation can be utilized to illustrate such a phenomenon. A higher loading rate means a shorter duration on piezoceramic materials. Hence, elastic deformation dominates in the loading stage and it recovers quickly during unloading due to a higher loading rate. There is little creep deformation due to the short duration of an applied stress. Therefore, a good piezoelectric effect can be maintained during cyclical loading under a higher loading rate. Thus, impact loads are preferred for power generation materials as they can generate stable and continuous power [6, 7].

3.4. Microstructure Analysis. Small pieces cut from the specimen that experienced cyclic loading were examined by SEM and XRD, respectively. A tight grain structure was observed with microvoids due to preparation of piezoelectric ceramics before compression tests (see Figure 11(a)). After compression, the grain gaps were formed and grains were debonded near voids. Further, some grains were crushed due

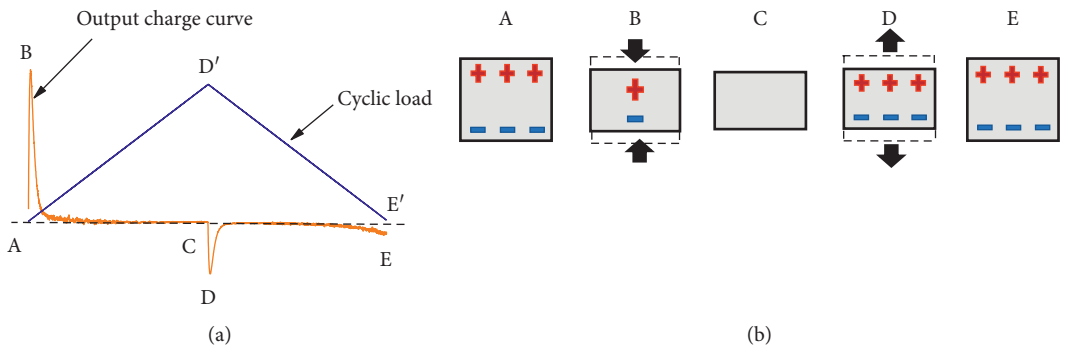

Figure 8: Diagram of piezoelectric effect under a triangle cyclic load. (a) The output charge induced by a cyclic load and (b) charges transferring due to applied uniaxial load.

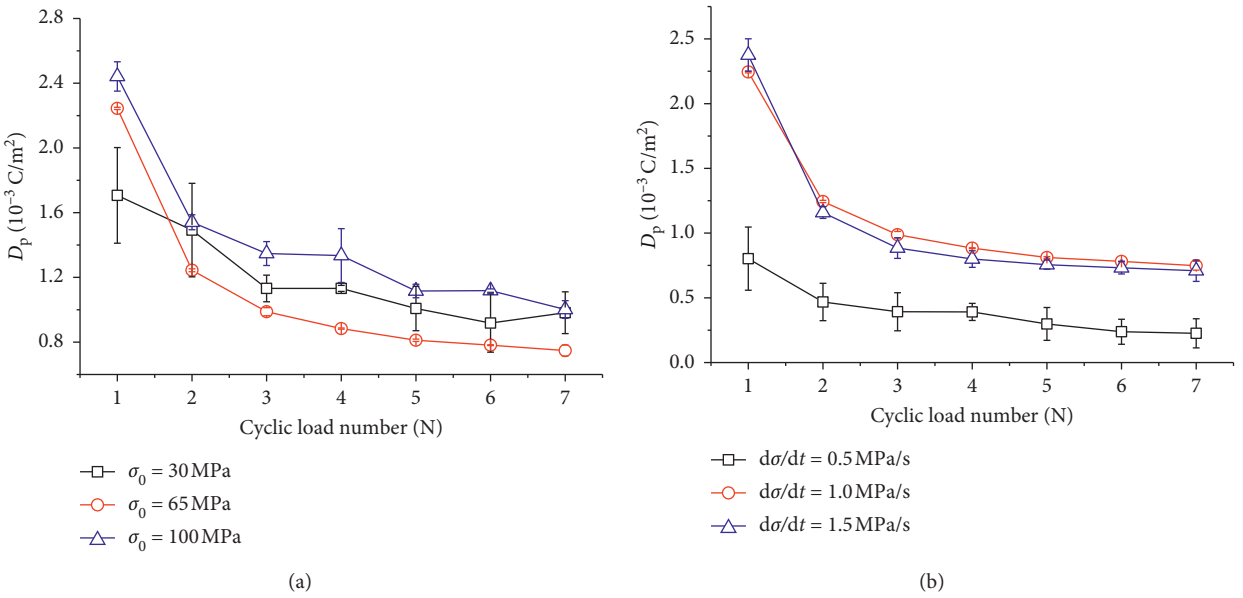

Figure 9: D_p versus the case with cyclic load number at (a) dσ/dt = 1.0 MPa/s and (b) σ_0 = 65 MPa.

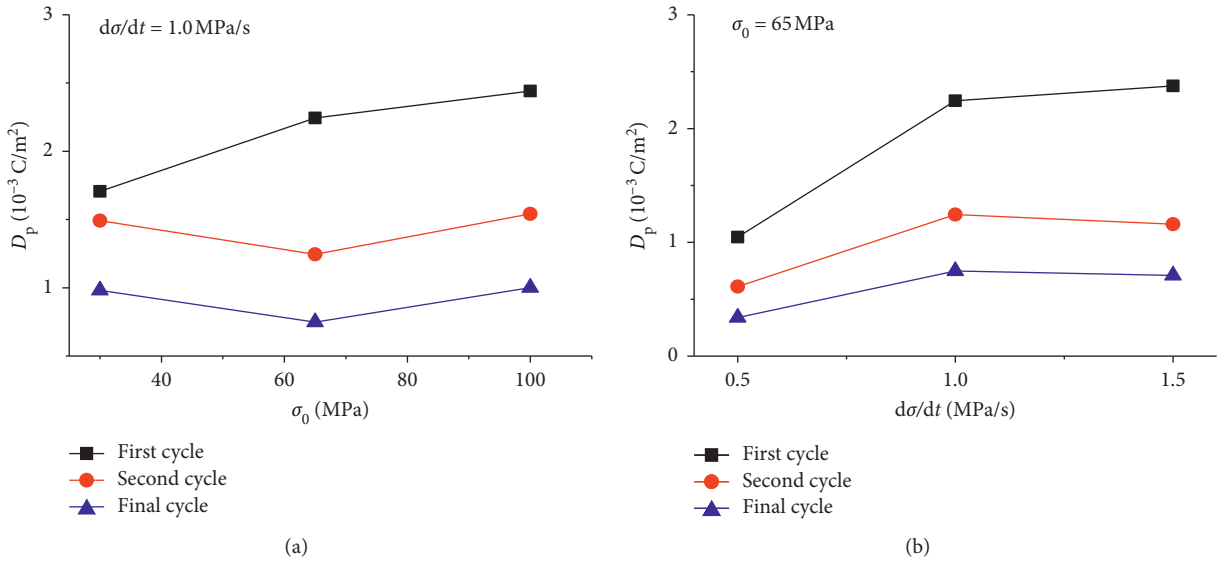

Figure 10: D_p versus the case with (a) σ_0 and (b) dσ/dt during the 1st, 2nd, and final cycles.

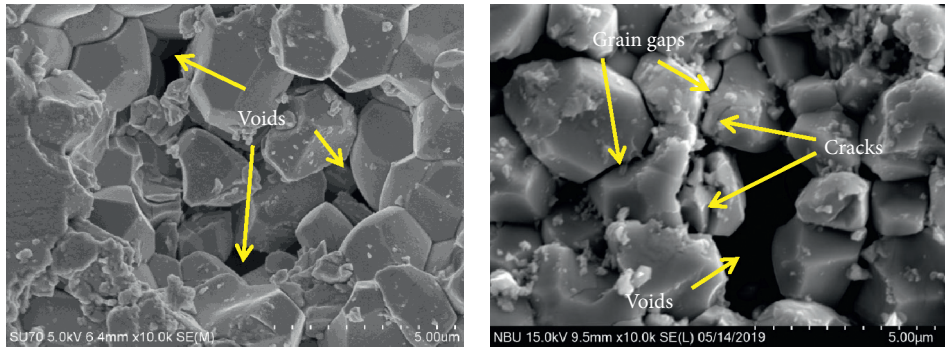

(a) (b)

Figure 11: SEM photographs of microstructure in P51 (a) before and (b) after compression.

to the nucleation and propagation of microcracks on the grain surface (shown in Figure 11(b)).

Dai and Guo [30] found that stress at the edge of an elliptical hole in a piezoelectric body was 1.574–6.164 times that of the average stress when the ratio of short to long axis of an elliptic hole was between 3 and 1/3. Therefore, stress at the edge of the elliptical hole reached 47.22–184.92 MPa under a stress of 30 MPa, which reached and even exceeded the critical stress of domain switching [12]. Hence, domain switching localized at the edge of microvoids, as well as grains that were debonded and crushed, could be all attributed to the effect of stress concentration.

Subsequently, the X-ray diffraction was conducted in order to observe the variation of the intensity of the two peaks at about 45 degrees induced by domain switching. According to Friedeld's principle [31], the content of *a* axis and *c* axis domain, which are parallel and perpendicular to the surface of the specimen, respectively, can be characterized by the peak intensities of (002) and (200) measured by XRD. Therefore, ferroelectric 90° domain switching can be analyzed by the variation of the peak intensity ratio of (002) to (200) after each cyclic load. Hence, the percentage of domain switching after test can be expressed as [32]

$$P(\%) = \frac{R_0 - R_i}{R_0\left(1 + \left(\left|F_{002}\right|^2 / \left|F_{200}\right|^2\right) \times R_i\right)} \times 100\%, \tag{9}$$

where R_0 and R_i are the ratio of peak intensity of (002) to (200) before and after test, respectively, that is,

$$R_0 = \left(\frac{I'_{200}}{I'_{002}}\right), \qquad R_i = \left(\frac{I_{200}}{I_{002}}\right), \quad i = 1, 2, 3, \ldots, \tag{10}$$

where the subscripts 0 and i represent the cyclic load number.

According to literature [33], $|F_{002}|$ and $|F_{200}|$, denoted as the modulus of structure factor, can be obtained as

$$\left|F_{002}\right| = 85.7, \qquad \left|F_{200}\right| = 95.6. \tag{11}$$

Figures 12(a)~12(e) show the variation of peak intensity at about 45 degrees conducted by XRD before and after cyclic load. At last, by substituting (10 and 11) into (9), the percentage of domain switching (P (%)) after cyclic loading is listed in Table 2 and plotted in Figure 12(f). Figure 12(f) indicates that the variation of P thoroughly agrees with that of d_{33}.

3.5. Modeling the Evolution of Electrical Displacement and Energy Dissipation. As discussed above, the variation of the dissipated energy is similar to that of the peak electrical displacement with the increase of the cyclic number. As a consequence, more 90° domain switching stimulates a larger dissipated energy and a bigger peak electrical displacement at the initial cyclic loading. Both the dissipated energy and the peak electrical displacement drop close to a constant until the saturation of 90° domain switching. Therefore, the peak electrical displacement can be assumed as an exponential function with respect to the dissipated energy, which is written as

$$D_p = D_0 \cdot \left(1 - e^{\left(-W_d/b\right)}\right), \tag{12}$$

where D_p and W_d are the values of the peak electrical displacement and the dissipated energy, respectively. Here, the values of D_p and W_d were obtained from the experimental data. That is, there are only two parameters that need to be determined in (12). Through curve fitting, the values of D_0 and b were obtained and listed in Table 3. By substituting D_0 and b into (12), a model that simulated the evolution of the peak electrical displacement, based on the dissipated energy, was setup, as shown in Figure 13.

Now let us discuss the physical meaning of D_0 and b. Equation (12) shows that the value of D_p must be less than that of D_0. That is, only when $W_d \longrightarrow \infty$, we have $D_p = D_0$. However, there is only one kind of lead zirconate-titanate ceramic material used in this paper, D_0, got by curve fitting at different stress amplitude and loading rate, can be averaged and fixed as $3.6\,10^{-3}$ C/m^2. Another parameter, b, is the slope of the straight line shown in Figure 13. As a result, (12) can be utilized to simulate the evolution of D_p variation with W_d approximately in different stress amplitude and loading rate (see Figure 13).

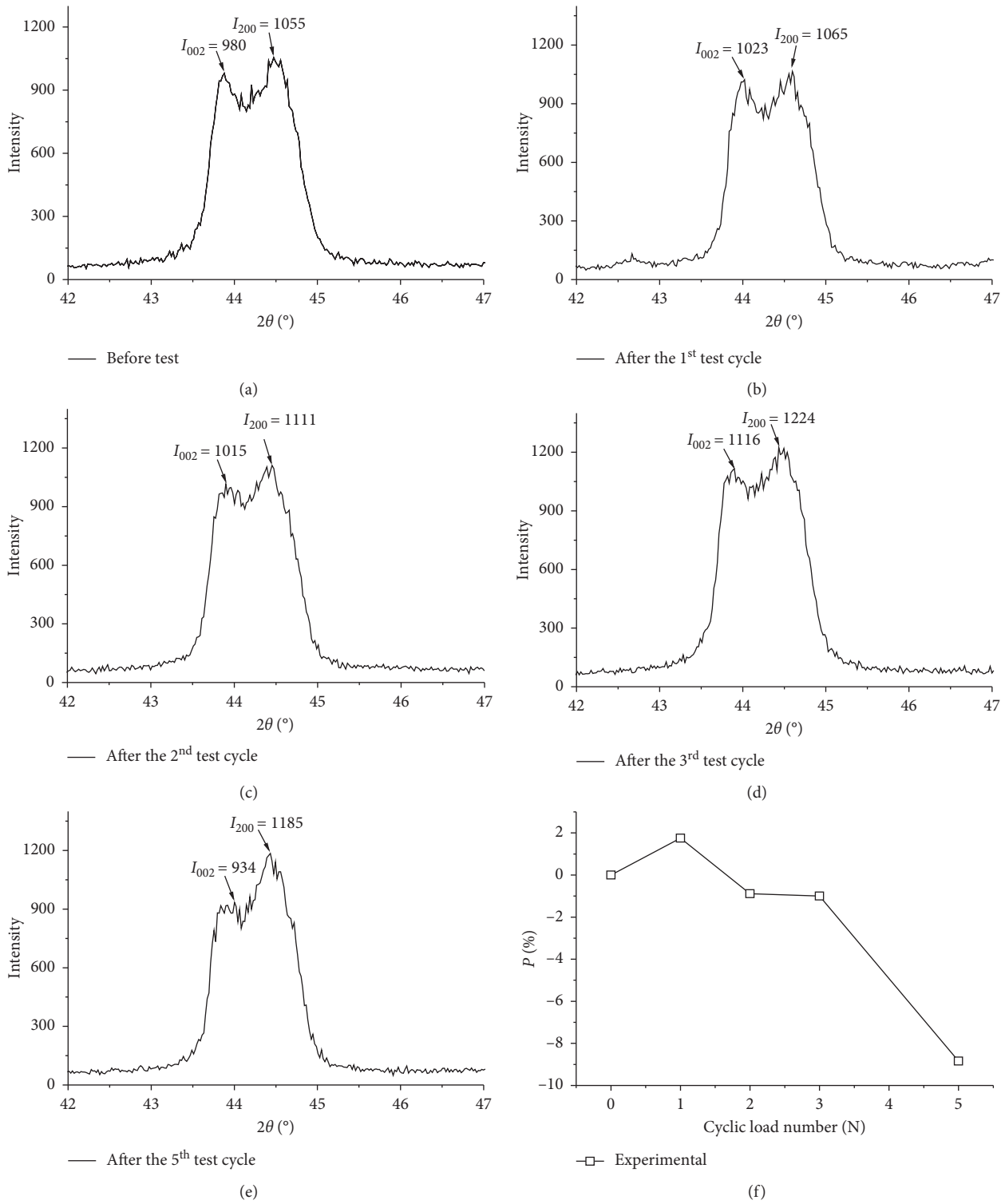

FIGURE 12: (a)~(e) X-ray diffraction pattern of P51at the cyclic number of 0, 1st, 2nd, 3rd, and 5th at $\sigma_0 = 65$ MPa and $d\sigma/dt = 1.0$ MPa/s, respectively. (f) Percentage of domain switching versus that with cyclic load number.

Table 2: The percentage of domain switching after cyclic loading.

Cyclic load number (N)	0	1	2	3	5
Stress amplitude/loading rate (MPa)/(MPa/s)	65/1.0	65/1.0	65/1.0	65/1.0	65/1.0
R	1055/980	1065/1023	1111/1015	1224/1116	1185/934
P (%)	0	1.75	−0.89	−1.00	−8.84

Table 3: The parameters of D_0 and b fitted by using (12).

Loading rate (MPa/s)	Stress amplitude (MPa)	D_0 (10^{-3} C/m^2)	b (10^{-3} J/mm^3)
1.0	30	3.6	0.087
1.0	65	3.6	0.359
1.0	100	3.6	0.358
0.5	65	3.6	1.083
1.5	65	3.6	0.178

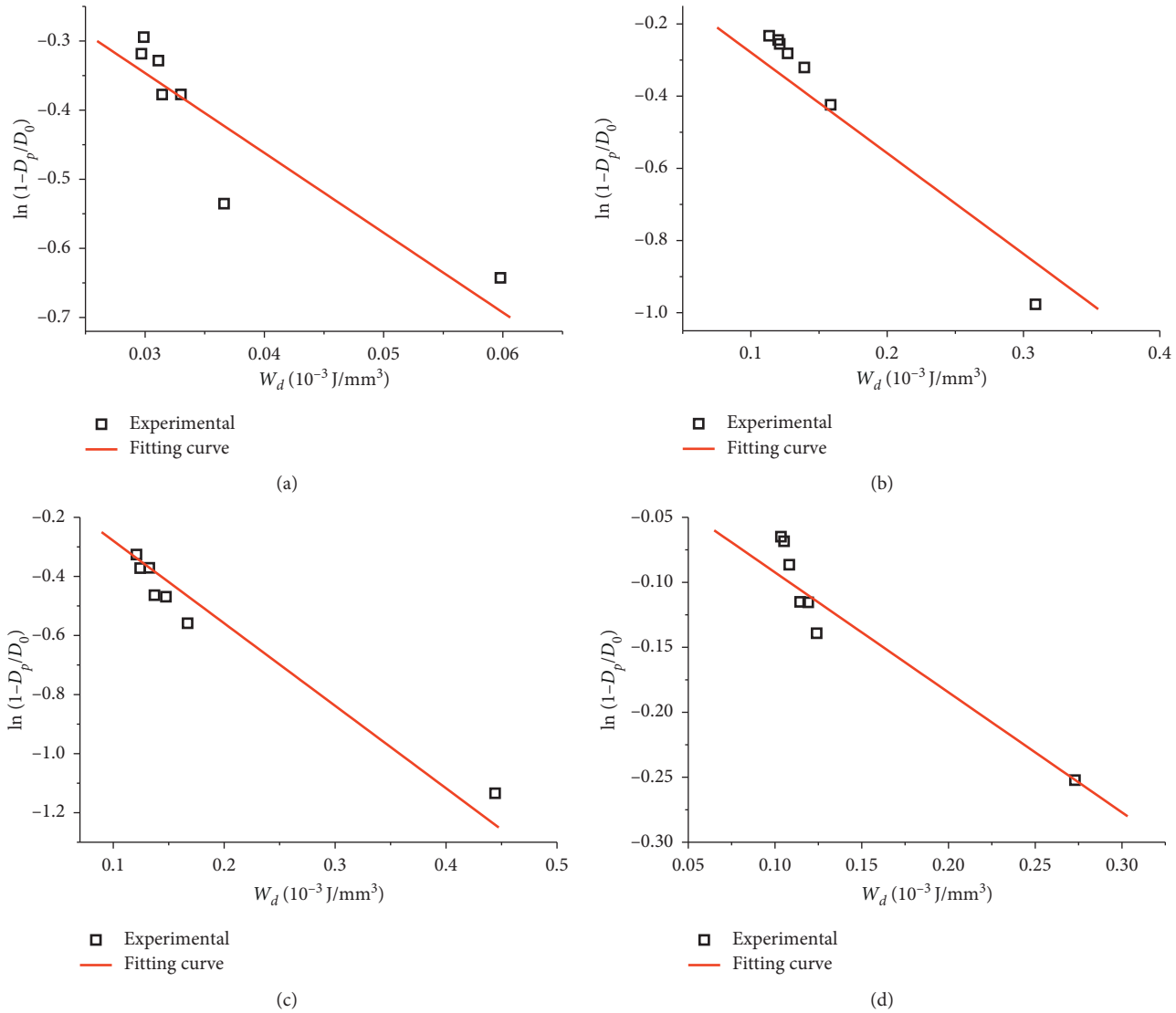

Figure 13: Continued.

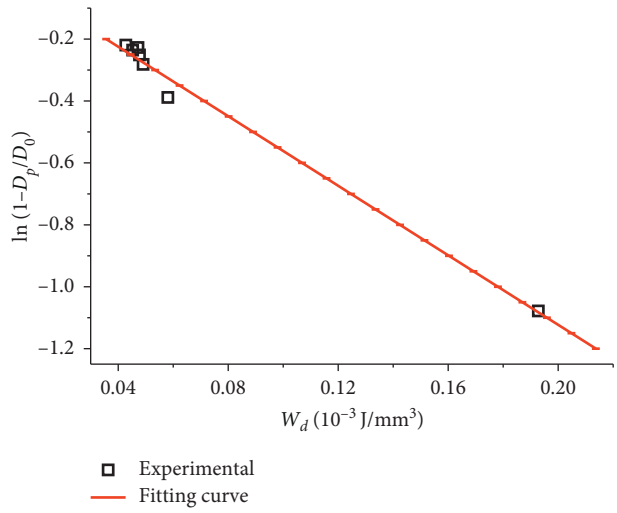

(e)

Figure 13: Electrical displacement versus dissipated energy. (a) $\sigma_0 = 30$, $d\sigma/dt = 1.0$. (b) $\sigma_0 = 65$, $d\sigma/dt = 1.0$. (c) $\sigma_0 = 100$, $d\sigma/dt = 1.0$. (d) $\sigma_0 = 65$, $d\sigma/dt = 0.5$. (e) $\sigma_0 = 65$, $d\sigma/dt = 1.5$ (in the units of MPa and MPa/s, respectively).

4. Conclusions

In this paper, a cyclical loading experiment of uniaxial compression was carried out to investigate the evolution of the peak electrical displacement based on the dissipated energy of lead zirconate-titanate ceramics (P51) under different stress amplitude and loading rate. The main conclusions can be drawn as follows:

(1) An exponential function model was proposed to simulate the degradation of the peak electrical displacement related to the energy dissipation of lead zirconate-titanate ceramic materials

(2) Degradation of the peak electrical displacement is attributed to the domain switching, which leads to the decrease of the piezoelectric coefficient by applied compression stress

(3) Percentage of domain switching can be calculated by the variation of the ratio of peak intensity (002) to (200) at about 45 degrees detected by XRD

(4) The energy dissipation of piezoceramics monotonously decreases with the loading rate, and the maximum reduction of the dissipated energy is 62.50% at $\sigma_0 = 65$ MPa

(5) The peak electrical displacement of piezoceramics monotonously increases with the loading rate, and the maximum increment is 127.01% at $\sigma_0 = 65$ MPa

Data Availability

The data used to support the findings of this study are included within the article.

Conflicts of Interest

The authors declare that there are no conflicts of interest regarding the publication of this paper.

Acknowledgments

This work was supported by the National Natural Science Foundation of China (NSFC) #11832013 and #11772164, the National Basic Research Program of China (973 Program), 2009CB623203, the Key Research Program of Society Development of Ningbo (2013C51007), and K.C. Wong Magna Fund in Ningbo University.

References

[1] M. Sun, W. J. Staszewski, and R. N. Swamy, "Smart sensing technologies for structural health monitoring of civil engineering structures," *Advances in Civil Engineering*, vol. 2010, Article ID 724962, 13 pages, 2010.

[2] D. Wang, J. Zhang, and H. Zhu, "Embedded electromechanical impedance and strain sensors for health monitoring of a concrete bridge," *Shock and Vibration*, vol. 2015, Article ID 821395, 12 pages, 2015.

[3] G. Wang, J. He, J. Liu, H. Sun, Z. Ding, and M. Zhang, "Safety verification of interconnected hybrid systems using barrier certificates," *Mathematical Problems in Engineering*, vol. 2016, Article ID 4149059, 10 pages, 2016.

[4] M. M. S. Dezfouli, M. R. Hassan, M. H. Ruslan, S. Mat, and B. Bakhtyar, "Experimental and theoretical investigations of the impact localization of a passive smart composite plate fabricated using piezoelectric materials," *Advances in Materials Science and Engineering*, vol. 2013, Article ID 326713, 12 pages, 2013.

[5] A. Sambri, D. Isarakorn, A. Torres-Pardo et al., "Epitaxial piezoelectric $Pb(Zr_{0.2}Ti_{0.8})O_3$ thin films on silicon for energy harvesting devices," *Smart Materials Research*, vol. 2012, Article ID 426048, 7 pages, 2012.

[6] Y. Tian, G. Li, Z. Yi, J. Liu, and B. Yang, "A low-frequency MEMS piezoelectric energy harvester with a rectangular hole based on bulk PZT film," *Journal of Physics and Chemistry of Solids*, vol. 117, pp. 21–27, 2018.

[7] J. Chen, Q. Qiu, Y. Han, and D. Lau, "Piezoelectric materials for sustainable building structures: fundamentals and

applications," *Renewable and Sustainable Energy Reviews*, vol. 101, pp. 14–25, 2019.

[8] I. J. Fritz, "Stress effects in two modified lead zirconate titanate ferroelectric ceramics," *Journal of Applied Physics*, vol. 50, no. 8, pp. 5265–5271, 1979.

[9] H. Cao and A. G. Evans, "Nonlinear deformation of ferroelectric ceramics," *Journal of the American Ceramic Society*, vol. 76, no. 4, pp. 890–896, 1993.

[10] C. S. Lynch, "The effect of uniaxial stress on the electromechanical response of 8/65/35 PLZT," *Acta Materialia*, vol. 44, no. 10, pp. 4137–4148, 1996.

[11] J. Fan, W. A. Stoll, and C. S. Lynch, "Nonlinear constitutive behavior of soft and hard PZT: experiments and modeling," *Acta Materialia*, vol. 47, no. 17, pp. 4415–4425, 1999.

[12] J. M. Calderon-Moreno, "Stress induced domain switching of PZT in compression tests," *Materials Science & Engineering A (Structural Materials: Properties, Microstructure and Processing)*, vol. 315, no. 1-2, pp. 227–230, 2000.

[13] M. Algueró, B. L. Cheng, F. Guiu, M. J. Reece, M. Poole, and N. Alford, "Degradation of the d_{33} piezoelectric coefficient for PZT ceramics under static and cyclic compressive loading," *Journal of the European Ceramic Society*, vol. 21, no. 10-11, pp. 1437–1440, 2001.

[14] M. Okayasu, G. Ozeki, and M. Mizuno, "Fatigue failure characteristics of lead zirconate titanate piezoelectric ceramics," *Journal of the European Ceramic Society*, vol. 30, no. 3, pp. 713–725, 2010.

[15] D. Fang and C. Li, "Nonlinear electric-mechanical behavior of a soft PZT-51 ferroelectric ceramic," *Journal of Materials Science*, vol. 34, no. 16, pp. 4001–4010, 1999.

[16] M. H. Lente and J. A. Eiras, "Interrelationship between self-heating and ferroelectric properties in PZT ceramics during polarization reorientation," *Journal of Physics: Condensed Matter*, vol. 12, no. 27, pp. 5939–5950, 2000.

[17] D. Zhou and M. Kamlah, "Room-temperature creep of soft PZT under static electrical and compressive stress loading," *Acta Materialia*, vol. 54, no. 5, pp. 1389–1396, 2006.

[18] K. G. Webber, E. Aulbach, T. Key, M. Marsilius, T. Granzow, and J. Rödel, "Temperature-dependent ferroelastic switching of soft lead zirconate titanate," *Acta Materialia*, vol. 57, no. 15, pp. 4614–4623, 2009.

[19] S. Pojprapai, Z. Luo, B. Clausen et al., "Dynamic processes of domain switching in lead zirconate titanate under cyclic mechanical loading by in situ neutron diffraction," *Acta Materialia*, vol. 58, no. 6, pp. 1897–1908, 2010.

[20] S. Hackemann and W. Pfeiffer, "Domain switching in process zones of PZT," *Journal of the European Ceramic Society*, vol. 23, no. 1, pp. 141–151, 2003.

[21] A. E. Glazounov, H. Kungl, J.-T. Reszat et al., "Contribution from ferroelastic domain switching detected using X-ray diffraction toR-curves in lead zirconate titanate ceramics," *Journal of the American Ceramic Society*, vol. 84, no. 12, pp. 2921–2929, 2001.

[22] F. Meschke, O. Raddatz, A. Kolleck, and G. A. Schneider, "R-curve behavior and crack-closure stresses in barium titanate and (Mg, Y)-PSZ ceramics," *Journal of the American Ceramic Society*, vol. 83, no. 2, pp. 353–361, 2000.

[23] A. B. K. Njiwa, D. C. Lupascu, and J. Rödel, "Crack tip switching zone in ferroelectric ferroelastic materials," *Acta Materialia*, vol. 52, no. 16, pp. 4919–4927, 2004.

[24] G. A. Schneider, "Influence of electric field and mechanical stresses on the fracture of ferroelectrics," *Annual Review of Materials Research*, vol. 37, no. 1, pp. 491–538, 2007.

[25] H. Duan and Y. Yang, "Deformation and dissipated energy of sandstone under uniaxial cyclic loading," *Geotechnical and Geological Engineering*, vol. 36, no. 1, pp. 611–619, 2018.

[26] Y. A. Genenko, J. Glaum, M. J. Hoffmann, and K. Albe, "Mechanisms of aging and fatigue in ferroelectrics," *Materials Science and Engineering: B*, vol. 192, pp. 52–82, 2015.

[27] A. G. Luchaninov, A. V. Shil'nikov, L. A. Shuvalov, and V. A. Malyshev, "The effect of mechanical stress on the properties of electrically depolarized piezoelectric ceramics," *Ferroelectrics*, vol. 145, no. 1, pp. 235–239, 1993.

[28] T. Feit, D. Munz, and G. Thun, "Dielectric parameters of a soft PZT under mechanical loading," *Journal of Materials Science Letters*, vol. 21, pp. 849–852, 2002.

[29] Z. J. Li, D. Zhang, and K. R. Wu, "Cement matrix 2-2 piezoelectric composite- part 1. Sensory effect," *Materials and Structures*, vol. 34, no. 8, pp. 506–512, 2001.

[30] L. C. Dai and W. L. Guo, "On the problem of piezoelectric solid with an elliptic hole," *Chinese Journal of Theoretical and Applied Mechanics*, vol. 36, pp. 224–228, 2004, in Chinese.

[31] R. W. James, *The Optical Principles of the Diffraction of X-Rays*, Ox Bow Press, Woodbridge, CT, USA, 1982.

[32] X. W. Zhang, C. Lei, and K. P. Chen, "Ferroelectric 90° domain evaluation in tetragonal $Pb(Mg_{1/3}Nb_{2/3})O_3$–$PbTiO_3$ ceramics," *Journal of the American Ceramic Society*, vol. 88, no. 2, pp. 335–338, 2010.

[33] Y. Y. Wang, *In-situ XRD Measurement System for Ferroelectric Domain Switching and its Application*, Ximen University, Xiamen, China, 2006.